JOURNAL OF EXPERIMENTAL AND THEORETICAL PHYSICS, 2025, Vol. 167, No. 2, pp. 260–271



# THERMOTROPIC PHASE TRANSITION SOLID–LIQUID AT THE OIL–WATER INTERFACE

© 2025 A. M. Tikhonov

*Kapitza Institute for Physical Problems Russian Academy of Sciences, Moscow, Russia*

*e-mail: tikhonov@kapitza.ras.ru*

Received September 19, 2024

Revised October 15, 2024

Accepted October 15, 2024

**Abstract**. The paper systematizes both the data of interfacial tension and X-ray scattering measurements using synchrotron radiation in the vicinity of the solid-liquid thermotropic phase transition in a soluble adsorption film of triacontanoic acid at the n-hexane–water interface. With increasing temperature, the structure of the film, with a thickness of 200 to 400 Å, is reconstructed in two stages. First, at a temperature of $T_c$, the solid Gibbs monolayer (area per molecule $A = (18.8 \pm 0.5)$ Å$^2$) melts sharply, and the subsequent decrease in the film thickness to a value of $36 \pm 3$ Å into one liquid monolayer ($A = (23 \pm 1)$ Å$^2$) occurs in a wide temperature range of $\geq 20$ K. The excess electron density observed in the solid phase of the monolayer is, in our opinion, associated with the addition of electrolyte ions and water molecules to the polar group of the lipid. According to experimental data, the transition temperature $T_c$, the transition enthalpy and the structure of the adsorption film of carboxylic acid depend on the composition of the background electrolyte in the aqueous subphase.

**Keywords**: *x-ray scattering*, *x-ray reflectivity*, *liquid-liquid interface*, *adsorption*, *thin films*

**DOI:** 10.31857/S004445102502e129

## 1. INTRODUCTION

A soluble Gibbs film of a surfactant at an interface can be considered as a two-dimensional thermodynamic system whose physical parameters are fundamentally different from the "bulk" characteristics of both the amphiphilic substance and the solvent [1, 2]. Such films often play a key role in various technological applications. For example, the properties of lubricating oils in micron-sized layers of friction triads can be explained by the formation of structured "boundary" layers of liquid with a "different" viscosity, different from the bulk viscosity [3]. Moreover, many authors discuss the efficiency of oil-technological processes associated with the thermotropic and lyatropic properties of adsorption films of impurity substances in water-oil emulsions [4, 5].

In a heterogeneous oil–water system, the isotropy of the bulk phases is violated at the interface and, for reasons of symmetry, the existence of a polarization vector perpendicular to its surface is allowed. Due to

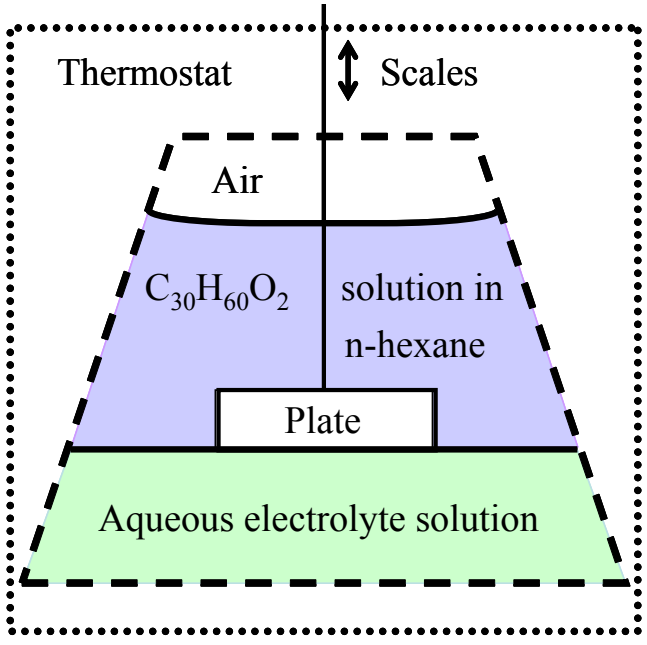


**Fig. 1.** Interfacial tension measurement scheme

microscopic interactions of the components of the bulk phases in the surface electric double layer [6, 7], the phase boundary can be strongly polarized, and as a result, a non-uniform and even anisotropic (in the interface plane) transition layer can arise on it. For example, a thermotropic solid–liquid phase transition is observed on the surface of a liquid high-molecular saturated hydrocarbon at a temperature several degrees higher than the bulk crystallization temperature [8, 9], in connection with which a number of authors have long discussed the possibility of the existence of a similar phase transition of "freezing" of the oil–water interface [10–13]. Later, in work [14], it was reported about observing such a transition in soluble films of triacontanoic acid (acid-$C_{30}$) at the n-hexane–water interface.

This paper systematizes the results of measurements of interfacial tension and X-ray scattering using hard synchrotron radiation in the vicinity of this phase transition, published earlier, and presents new ones. According to experimental data, the transition temperature $T_c$, transition enthalpy $\Delta H$ and structure of adsorption films of acid-$C_{30}$ depend on the composition of the background electrolyte in the volume of the aqueous subphase.

## 2. THE EXPERIMENT

Samples of the macroscopically flat n-hexane–water interface were studied in a thermostatted cell with geometric dimensions of the interface 75 mm 150 mm in accordance with the procedure described in [15]. The systems studied were those with a fixed volume concentration of acid-$C_{30}$ in n-hexane (upper phase) $c \approx 0.2$ mmol/kg ($\approx 3 \cdot 10^{-5}$) and an amount of substance sufficient to cover the interface with a layer of $\sim 10^3$ acid monolayers. Triacontanoic acid $C_{30}H_{60}O_2$ and n-hexane were purchased from Sigma-Aldrich. The saturated hydrocarbon $C_6H_{14}$ with a boiling point of $T_b \approx 342$ K and a density at 298 K $\approx 0.65$ g/cm$^3$ was preliminarily purified by multiple filtration in a chromatographic column [16]. Acid-$C_{30}$ (molar mass $\approx 453$ g/mol) was purified twice by recrystallization at room temperature from a supersaturated solution in n-hexane, which was prepared by dissolving the acid in the latter at $T \geq 60$ °C [17].

In the first group of samples (system I), a solution of sulfuric acid (pH $\approx 2$) in deionized water (Barnstead, NanoPureUV) with a volume of $\sim 100$ ml was used as the lower bulk phase, in which acid-$C_{30}$ is practically insoluble. In the second group of samples (system II), a solution of KOH in deionized water with a pH of $\approx 10$ was used as the lower bulk phase. In the third group of samples (system III), the aqueous bulk phase, in addition to KOH with a pH of $\approx 10$, contained ethylenediaminetetraacetic acid (EDTA) at a concentration of $\sim 2.5$ g/l. The tetrabasic carboxylic acid EDTA $(HOOCCH_2)_2N(CH_2)_2N(CH_2COOH)_2$ is insoluble in n-hexane, but dissolves in alkalis [18]. In the electrolyte solution, EDTA forms stable complexes with metal cations.

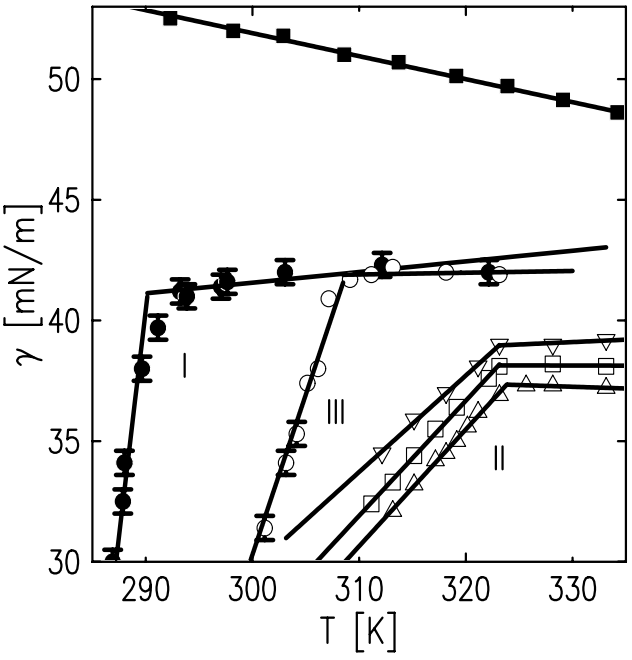


**Fig. 2.** Temperature dependences of the interfacial tension $\gamma(T)$ of the n-hexane–water interface for systems with different compositions of the background electrolyte: points I – sulfuric acid solution (pH $\approx 2$) with $T_c \approx 298$ K; II – potassium hydroxide solution (triangles correspond to pH=9.7, squares – pH=10.1, and inverted triangles – pH=10.5). The break point corresponds to $T_c \approx 323$ K; III – potassium hydroxide and ethylenediaminetetraacetic acid solution (pH $\approx 10$) with $T_c \approx 308$ K. The volume concentration of acid-$C_{30}$ in the hydrocarbon is $c \approx 0.2$ mmol/kg ($\approx 3 \cdot 10^{-5}$). Black squares show the temperature dependence $\gamma(T)$ for the pure n-hexane–water interface. Lines – fitting $\gamma(T)$ by linear functions

Finally, to prevent the formation of gas bubbles at the interface, the sample was subjected to "annealing": the temperature of the liquids in the cell was brought to $\sim 60$ °C, and then dropped below $T_c$. Then, the samples were brought to equilibrium for at least 12 hours after the change in cell temperature.

The interfacial tension of all samples was measured using the Wilhelmy method using a chromatographic paper plate (Wattman) with a length of $L \approx 10$ mm and a width of $\approx 5$ mm [19]. The plate, completely immersed in the oil phase, is attached to a thin ($\approx 0.25$ mm in diameter) platinum wire passing through holes in the thermostat lids and the cell hatch (Fig. 1). The maximum change in the weight of the plate $\Delta F$ during its slow pull out of the lower phase is recorded in the experiment using an electric balance (NIMA PS-2). Fig. 2 shows the dependences $\gamma(T) = \Delta F / 2L$ for all groups of samples that have a feature (kink) at the phase transition temperature $T_c$. The change in the slope $\gamma(T)$ is associated with a change in the surface enthalpy $\Delta H = -T_c \Delta(\partial\gamma / \partial T)_{p,c}$ during the phase transition, where $p$ is the pressure. Points I correspond to the first group of samples with pH $\approx 2$, the second group is presented for systems with different pH levels (II): circles – pH = 9.7, light squares – pH = 10.1, and triangles – pH = 10.5. Finally, the dependencies $\gamma(T)$ for the third type of samples correspond to circles III. The value $\Delta H$ for the first group is $1.1 \pm 0.1$ J/m$^2$, for the second $0.13 \pm 0.02$ J/m$^2$, and for the third $0.4 \pm 0.04$ J/m$^2$ (see Table). In Fig. 2, the black squares show the temperature dependence $\gamma(T)$ for the pure n-hexane–water interface. The lines are the fitting $\gamma(T)$ by a linear function.

**Table.** System parameters

| System | $T_c$ (K) | $\Delta H$ (J/m$^2$) | pH |
|---|---|---|---|
| I | 291 | $1.1 \pm 0.1$ | 2 |
| II | 323 | $0.13 \pm 0.02$ | 10 |
| III | 308 | $0.4 \pm 0.04$ | 10 |

The structure of the n-hexane–water interface was studied by X-ray reflectometry and diffuse scattering at the X19C station of the NSLS synchrotron [20]. A focused monochromatic beam with an intensity of approximately $10^{11}$ f/s and a photon energy of about 15 keV ($\lambda = 0.825 \pm 0.002$ E) was used in the experiments. The design of the spectrometer at this station allows structural studies of both the surface of solids [21] and the gravitationally oriented surfaces of liquids [22] and liquid–liquid interfaces [23].

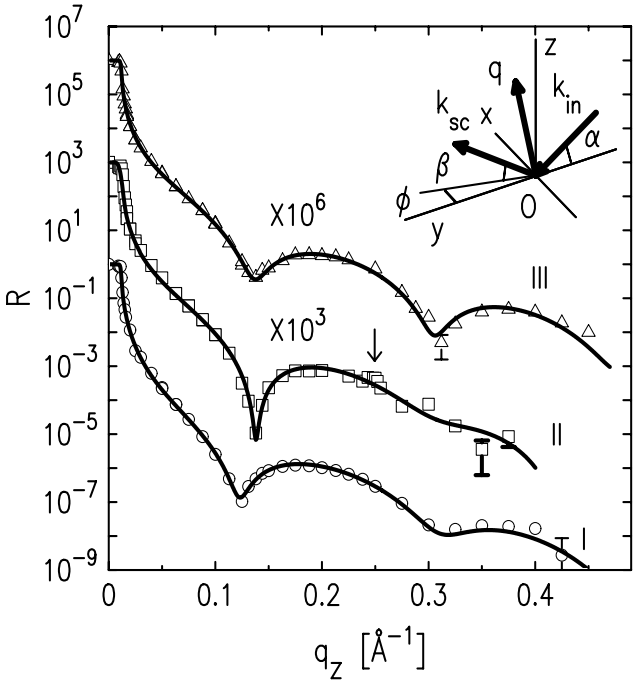


**Fig. 3.** Reflectivity $R$ for the low-temperature phase of the acid-$C_{30}$ adsorption film at the n-hexane–water interface for systems with different background electrolyte compositions: circles I – sulfuric acid solution (pH $\approx 2$) at $T \approx 288$ K; squares II – potassium hydroxide solution (pH=10) at $T \approx 320$ K; triangles III – potassium hydroxide and ethylenediaminetetraacetic acid solution (pH $\approx 10$) at T $\approx 303$ K. Lines – monolayer model (11). The arrow marks the position of the peak on curve II (see Fig. 8). Inset: scattering kinematics is described in a coordinate system in which the plane $xy$ coincides with the boundary between the monolayer and water, the axis $Ox$ is perpendicular to the beam direction, and the axis $Oz$ is directed along the normal to the surface opposite to gravity

The kinematics of surface scattering at a macroscopically flat interface (see inset in Fig. 3) oriented by gravity is conveniently described in a coordinate system in which the origin $O$ lies at the center of the illuminated region. The plane $xy$ coincides with the interface, the axis $Ox$ is perpendicular to the beam direction, and the axis $Oz$ is directed along the normal to the surface opposite to gravity. In the experiment, the grazing angle $\alpha << 1$ and the scattering angle $\beta << 1$ are in the plane $yz$ and the angle in the plane $xy$ between the direction of the incident beam and the direction of scattering is $\phi \approx 0$. Let $\mathbf{k}_{in}$, $\mathbf{k}_{sc}$ be the wave vectors with the amplitude $k_0 = 2\pi / \lambda$ of the incident and scattered beams in the direction of the observation point, respectively. For specular reflection ($\alpha = \beta$, $\phi = 0$), the scattering vector $\mathbf{q} = \mathbf{k}_{in} - \mathbf{k}_{sc}$ is directed strictly along $Oz$, $q_z \approx 2k_0\alpha$. At $\alpha \neq \beta$ components $q$ in the plane of the interface

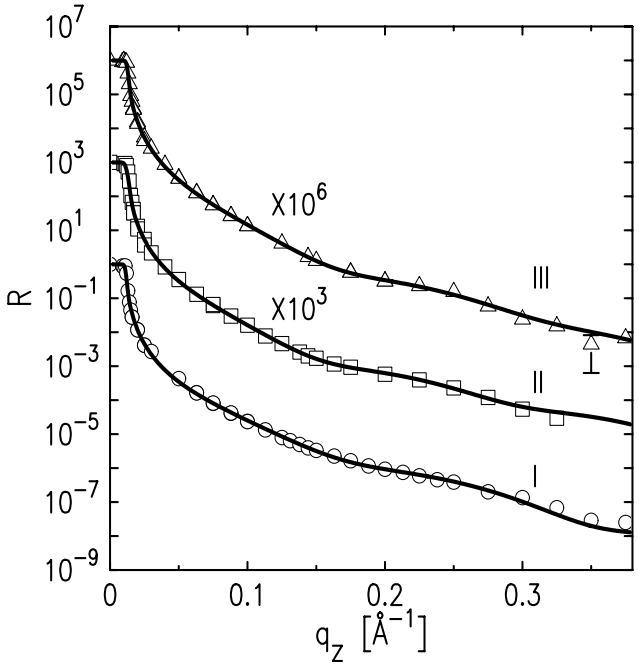


**Fig. 4.** Reflectivity $R$ for the high-temperature phase of the acid-$C_{30}$ adsorption film at the n-hexane–water interface for systems with different background electrolyte compositions: circles I – sulfuric acid solution (pH ≈ 2) at $T \approx 318$ K; squares II – potassium hydroxide solution (pH=10) at $T \approx 333$ K; triangles III – potassium hydroxide and ethylenediaminetetraacetic acid solution (pH ≈ 10) at $T \approx 327$ K. Lines – monolayer model (11)

$q_x \approx k_0\phi$ and $q_y \approx k_0(\alpha^2 - \beta^2)/2$, and component $q_z \approx k_0(\alpha + \beta)$.

Figs. 3 and 4 show the dependences $R(q_z)$ for the low-temperature and high-temperature phases of the acid-$C_{30}$ adsorption film at the n-hexane–water interface, respectively, for systems with different background electrolyte compositions: circles I – sulfuric acid solution (pH ≈ 2) at $T \approx 288$ K and ≈ 318 K; squares II – potassium hydroxide solution (pH=10) at $T \approx 320$ K and ≈ 333 K; triangles III – potassium hydroxide and ethylenediaminetetraacetic acid solution (pH ≈ 10) at $T \approx 303$ K and ≈ 328 K.

At $q_z < q_c \approx 0.01$ Å$^{-1}$ the incident beam experiences total external reflection $R \approx 1$. Under normal conditions the value of the angle of total external reflection $\alpha_c$ ($q_c = 2k_0 \sin\alpha_c$) is determined by the difference $\Delta\rho \approx 0.11\ e^-/\text{Å}^3$ in the volume electron concentrations in water $\rho_w \approx 0.333\ e^-/\text{Å}^3$ and n-hexane $\rho_h \approx 0.226\ e^-/\text{Å}^3$ ($\approx 0.680\rho_w$), $\alpha_c = \lambda\sqrt{r_e\Delta\rho/\pi} \approx 10^{-3}$ rad, where $r_e = 2.814 \cdot 10^{-5}$ Å is the classical electron radius. In the calculations, the dependence of the density of n-hexane and water on temperature was taken into account in the value of the optical parameter $\alpha_c$.

Figs. 5 and 6 show the normalized intensity of surface scattering $I_n$ at a fixed grazing angle $\alpha \approx 3.3 \cdot 10^{-3}$ rad (≈ 0.19°), respectively, for the low-temperature and high-temperature phases of the acid-$C_{30}$ adsorption film at the n-hexane–water interface for systems with different subphase compositions: circles I – sulfuric acid solution (pH ≈ 2) at $T \approx 285$ K and ≈ 334 K; squares II – potassium hydroxide solution (pH=10) at $T \approx 320$ K and ≈ 330 K; triangles III – potassium hydroxide and ethylenediaminetetraacetic acid solution (pH ≈ 10) at $T \approx 303$ K and ≈ 327 K.

Intensity $I_n(\beta) \equiv (I(\beta) - I_b)/I_0$ (normalization condition $I_n(\alpha) \equiv 1$), where $I_0$ is the intensity of the incident beam, which is controlled in the experiment immediately before the beam enters the cell; $I(\beta)$ is the number of photons specularly reflected and diffusely scattered by the surface in the illumination region at the center of the interphase boundary of the sample in the direction β, as well as photons scattered in the volume of n-hexane along the path to the boundary; $I_b$ is the number of photons scattered in the volume of n-hexane along the path to the boundary. The technique for obtaining scattering curves $I_n(\beta)$ is described in detail in [24].

In the diffuse scattering curves (Figs. 5 and 6), the most intense peak corresponds to specular reflection $\beta = \alpha$, and the peak in the diffuse background at $\beta \to 0$ corresponds to the angle of total external reflection $\alpha_c \approx 10^{-3}$ rad (≈ 0.05°) [25]. The interval of characteristic in-plane lengths involved in scattering is $2\pi/q_y \sim 10^{-5} - 10^{-6}$ m. The long-wave limit is set by the vertical resolution of the detector Δβ, and the short-wave limit is set by the maximum value of $\beta \sim 1.2 \cdot 10^{-2}$ rad (≈ 0.7°), at which it is still possible to separate the contributions of the surface and volume components to the scattering intensity.

Finally, when measuring the reflection coefficient $R$ as a function $q_z$, its values are averaged over a large illuminated surface area (~ 0.5 cm$^2$) with an incident beam height (> 5 μm) in the plane $yz$ and a width of ~ 2 mm in the plane of the interface. When measuring the scattering intensity $I(\beta)$, the vertical size of the incident beam with an angular divergence of $\Delta\alpha \approx 10^{-4}$ rad was ≈ 0.05 mm at the sample surface and was controlled by a double-slit collimator. The angular resolution of the detector in the plane of incidence $\Delta\beta = 2H_d/L_2 \approx 3 \cdot 10^{-4}$ rad

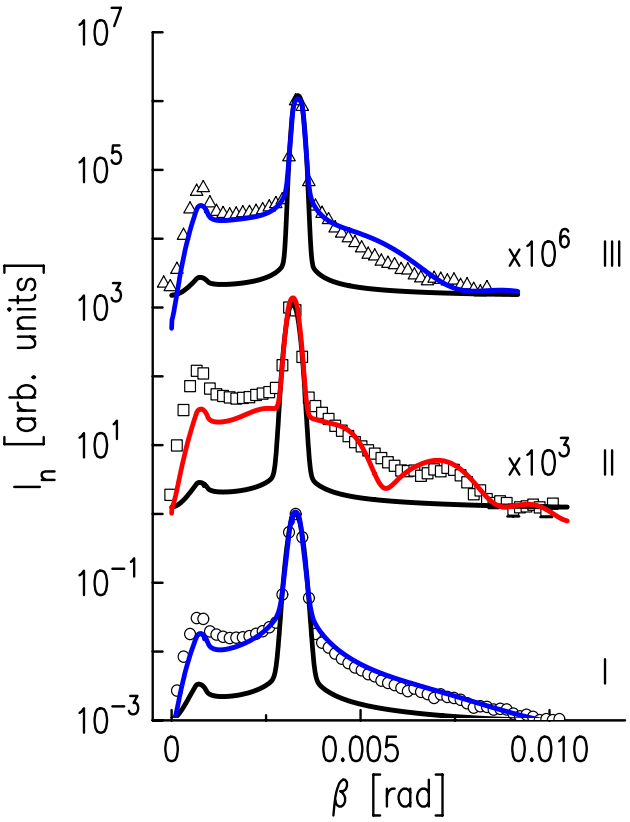


**Fig. 5.** Normalized intensity of surface scattering $I_n$ at a fixed grazing angle $\alpha \approx 3.3 \cdot 10^{-3}$ rad ($\approx 0.19°$) for the low-temperature phase of the acid-$C_{30}$ adsorption film at the n-hexane–water interface for systems with different background electrolyte compositions: circles I – sulfuric acid solution (pH $\approx$ 2) at $T \approx 285$ K; squares II – potassium hydroxide solution (pH=10) at $T \approx 320$ K; triangles III – potassium hydroxide and ethylenediaminetetraacetic acid solution (pH $\approx$ 10) at $T \approx 303$ K. Black lines – monolayer model (11), blue lines – three-layer model (13) of systems I and III, and the red line – model (14) of system II.

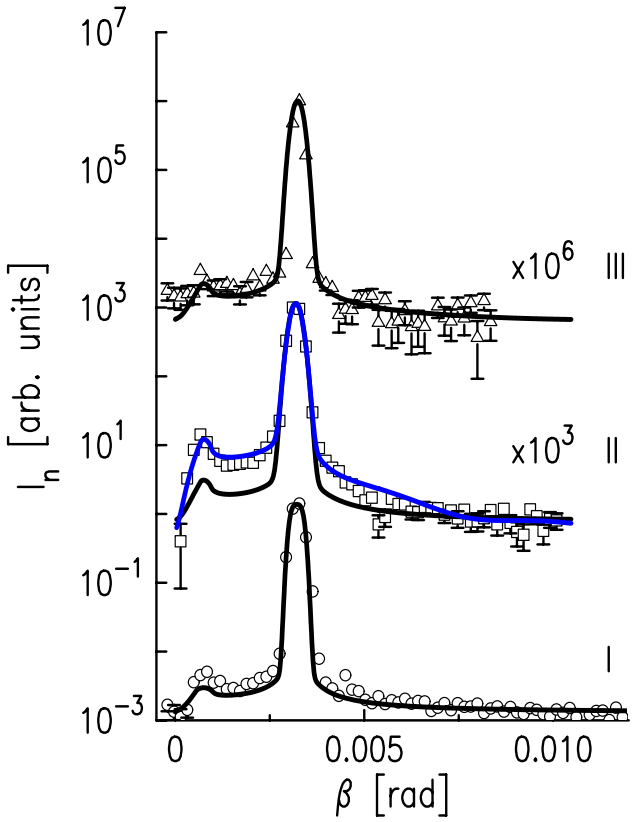


**Fig. 6.** Normalized intensity of surface scattering $I_n$ at a fixed grazing angle $\alpha \approx 3.3 \cdot 10^{-3}$ rad ($\approx 0.19°$) for the high-temperature phase of the acid-$C_{30}$ adsorption film at the n-hexane–water interface for systems with different background electrolyte compositions: circles I – sulfuric acid solution (pH $\approx$ 2) at $T \approx 334$ K; squares II – potassium hydroxide solution (pH=10) at $T \approx 330$ K; triangles III – potassium hydroxide and ethylenediaminetetraacetic acid solution (pH $\approx$ 10) at $T \approx 327$ K. Black lines – monolayer model (11), blue line – three-layer model (13)

is specified when measuring the diffuse scattering intensity by a slit in front of the detector with a gap of $2H_d = 0.2$ mm at a distance of $L_2 \approx 70$ cm from the sample center. When measuring the reflection coefficient $2H_d = 1.6$ mm ($\Delta\beta \approx 2 \cdot 10^{-3}$ rad). The distance from the collimator slit in front of the sample to the detector is $L_1 \approx 90$ cm. In the horizontal plane, the gap at all slits is $\approx 10$ mm, significantly exceeding the horizontal size of the incident beam $\sim 2$ mm ($\Delta\phi \approx 10^{-2}$ rad).

## 3. THEORY

In the distorted-wave Born approximation (DWBA), the scattering intensity $I_n$ of a monochromatic photon beam $I_0$ is the sum of diffuse scattering $I_{\text{diff}}$ and specular reflection $I_{\text{spec}}$ [26, 27]:

$$I_n = I_{\text{diff}} + I_{\text{spec}}. \quad (1)$$

The first term describes the non-specular scattering of photons by thermal fluctuations of the liquid surface (capillary waves) [28]:

$$I_{\text{diff}} \approx \frac{\lambda q_c^4}{512\pi^2}\frac{k_B T}{\Delta\alpha\gamma}\times$$
$$\times \int\limits_{\alpha-\frac{\Delta\alpha}{2}}^{\alpha+\frac{\Delta\alpha}{2}}\int\limits_{\beta-\frac{\Delta\beta}{2}}^{\beta+\frac{\Delta\beta}{2}} \frac{|T(\alpha)|^2 |T(\beta)|^2 |\Phi(\sqrt{q_z q_z^t})|^2}{\alpha\sqrt{q_y^2 + g\Delta\rho_m/\gamma}} d\beta d\alpha, \quad (2)$$

where $k_B$ is the Boltzmann constant, $g$ is the acceleration of gravity, $\gamma$ is the surface tension, $\Delta\rho_m \approx 0.34$ g/cm$^3$ is the difference in the density

of water and n-hexane, of the $z$-component of the scattering vector in the lower phase:

$$q_z^t = \frac{2\pi}{\lambda}\left[(\alpha^2 - \alpha_c^2)^{1/2} + (\beta^2 - \alpha_c^2)^{1/2}\right]. \quad (3)$$

$T(\theta)$ is the Fresnel transmission coefficient for the amplitude of a wave with polarization of synchrotron radiation in the plane of the interface

$$T(\theta) = \frac{2\theta}{\theta + (\theta^2 - \alpha_c^2)^{1/2}}, \quad (4)$$

and the structural factor of the interphase boundary

$$\Phi(q) = \frac{1}{\Delta\rho}\int_{-\infty}^{+\infty}\left\langle\frac{d\rho(z)}{dz}\right\rangle e^{iqz}dz \quad (5)$$

is determined by the Fourier transform of the derivative of the electron concentration $\rho(z)$ distribution along the illumination area $A_0$ averaged over $Oz$. Integration of expression (2) is carried out numerically [29, 30].

The intensity of specular reflection can be written as follows:

$$I_{spec} = f(\alpha,\beta)R(\alpha), \quad (6)$$

where the reflection coefficient is

$$R(\alpha) = \left|\frac{q_z - q_z^t}{q_z + q_z^t}\right|^2 \left|\Phi(\sqrt{q_z q_z^t})\right|^2, \quad (7)$$

calculated under the condition $\alpha \equiv \beta$ using expressions (3) and (5).

The hardware angular resolution $f(\alpha,\beta)$ function, taking into account the Gaussian distribution of beam intensity in the plane of incidence, has the following form [31]:

$$f(\alpha,\beta) = \frac{1}{2}\left[\mathrm{erf}\left(\frac{H + H_d}{\sqrt{2}L_1\Delta\alpha}\right) - \mathrm{erf}\left(\frac{H - H_d}{\sqrt{2}L_1\Delta\alpha}\right)\right], \quad (8)$$

where $H = (\beta - \alpha)L_2$.

Thus, the experimental dependences $R(q_z)$ and $I_n$ can be approximated by calculated curves, varying the parameters of the model electron concentration profile $\rho(z)$. The parameterization of the latter was carried out using the error function

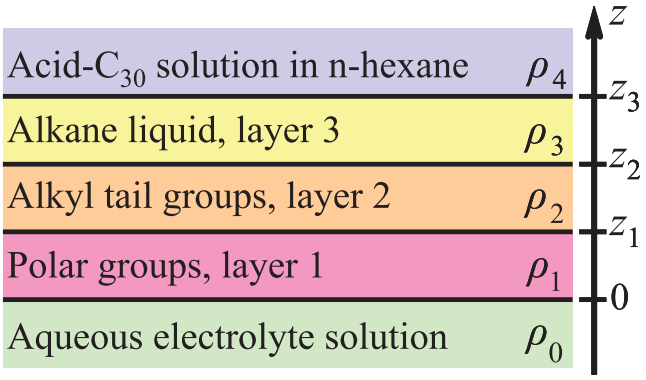


**Fig. 7.** Three-layer model of the adsorbed layer of triacontanoic acid $C_{30}H_{60}O_2$ at the n-hexane–water interface

$$\mathrm{erf}(x) = \frac{2}{\sqrt{\pi}}\int_0^x \exp(-y^2)dy, \quad (9)$$

which is used in the generally accepted theory of capillary waves [28].

## 4. SIMULATION RESULTS

The scattering data were analyzed using a three-layer model (see Fig. 7) of the n-hexane–water interphase boundary structure, where the near-surface structure is divided into layers of uniform density. Layer 1 contains hydrophilic polar groups -COOH, and layer 2 is formed from hydrophobic hydrocarbon (alkyl) tails -$C_{29}H_{59}$. These two layers describe the Gibbs monolayer of the acid-$C_{30}$. Layer 3 (alkane liquid) corresponds to a fairly extended layered (smectic) or disordered region of the structure, which, in our opinion, is formed from precipitated micelles of triacontanoic acid. The presence of this layer in the near-surface structure follows from the measurement data of the angular dependences of non-specular scattering. In the calculations $R(q_z)$ and $I_n$ to take into account the statistical properties of the roughness of the interlayer boundaries, the correlation function of heights, following from the standard theory of capillary waves [29], is used.

Thermal fluctuations of the liquid surface affect the observed structure of the surface layer. In this regard, two density profiles are distinguished – the real one and the proper one, not disturbed by the fluctuation collective motion of the liquid particles. The calculated value of the width of the blurring of boundaries by capillary waves

$$\sigma_R^2 \approx \frac{k_B T}{2\pi\gamma} \ln\left(\frac{Q_{max}}{Q_{min}}\right) \quad (10)$$

is determined by the short-wave limit in the spectrum of thermal fluctuations of the boundary $Q_{max} = 2\pi/a$ ($a \approx 10$ Å is the molecular radius in order of magnitude) and the angular resolution of the detector $Q_{min} = q_z^{max}\Delta\beta/2$ [30, 32–34].

In the first approximation, the dependencies $R(q_z)$ for all systems are described quite well by a qualitative two-layer model of a triacontanoic acid monolayer with the following structural factor [14]:

$$\Phi_m(q) = \frac{e^{-\sigma_R^2 q^2/2}}{\Delta\rho} \sum_{j=0}^{2} (\rho_{j+1} - \rho_j) e^{-iqz_j}, \quad (11)$$

where $z_0 = 0$, $\rho_0 \approx \rho_w$, and $\rho_3 = \rho_4 \approx \rho_h$. The thickness of layer 1 is equal to $L_1 = z_1$, and that of layer 2 is equal to $L_2 = z_2 - z_1$.

For the low-temperature solid phase, the electron concentrations $\rho_1 = (1.3 \pm 0.1)\rho_w$ and $\rho_2 = (0.98 \pm 0.02)\rho_w$ (where $\rho_w = 0.333$ $e^-/\text{Å}^3$ is the electron concentration in water under normal conditions) with the layer thicknesses $l_1 = z_1 - z_0 = 12 \pm 3$ Å and $l_2 = z_2 - z_1 = 29 \pm 2$ Å. The fitted values of the parameter $\sigma_R$ vary from 3.6 Å to 4.5 Å and coincide with the calculated value within the error limits. The total thickness of the monolayer is $l = 41 \pm 2$ Å.

In the high-temperature phase, the hydrophilic layer $\rho_1 = (1.12 \pm 0.02)\rho_w$ has a thickness of $l_1 = (18 \pm 2)$ Å. The electron concentration in the second layer of thickness $l_2 = 18 \pm 2$ Å is $\rho_1 = (0.77 \pm 0.02)\rho_w$. The fitted values of the parameter $\sigma_R$ vary from 3.6 Å to 4.0 Å and, within the error limits, coincide with the calculated values when taking into account the data for $\gamma(T)$.

Thus, all the dependencies $R(q_z)$ can be described by curves of sufficiently good quality within the framework of the two-layer model, the values of the parameters of which coincide within the errors for all systems. However, this model does not allow to describe the narrow interference maximum in the low-temperature phase for system II, which is present in the dependencies $R(q_z)$ at $q_z' \approx 0.25$ Å$^{-1}$ [35]. Observation of the latter indicates the presence of a significantly thicker structure with an estimated

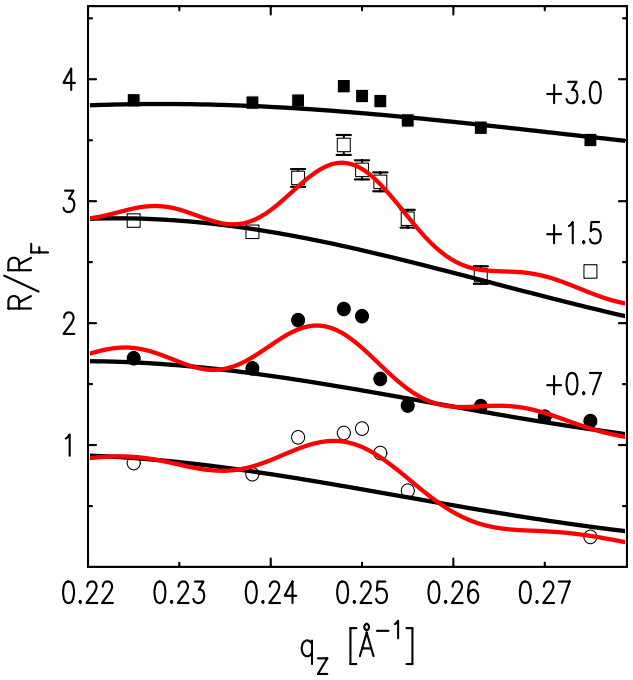


**Fig. 8.** Temperature dependence of the intensity $R(q_z)$, normalized to $R_F$: circles – 320.6 K; dots – 322.1 K; squares – 323.1 K; black squares – 323.5 K. Black lines – monolayer model (11); red lines – model (14) with the full width of the near-surface structure ~ 340 Å ($N = 8$) and $W \approx 50$ Å. For clarity, the numbers near the lines indicate the shift along the vertical axis

thickness $2\pi/\delta q_z' \sim 300$ Å, where the peak width is $\delta q_z' \simeq 0.02$ Å$^{-1}$. In Fig. 8, the temperature dependence $R(q_z)$, normalized to the Fresnel function

$$R_F(q_z) = \left(\frac{q_z - \sqrt{q_z^2 - q_c^2}}{q_z + \sqrt{q_z^2 - q_c^2}}\right)^2, \quad (12)$$

illustrates the disappearance of the interference maximum at $T \approx T_c$.

In addition, for all systems in the solid phase of the monolayer ($T < T_c$) the observed intensity $I_n$ is approximately two orders of magnitude higher than that calculated for the monolayer model. In the liquid phase of the monolayer ($T > T_c$) the intensity of the diffuse background $I_n(\beta)$ decreases with increasing temperature, but nevertheless, for system II, over the entire temperature range, it remains significantly higher than the prediction for model (11).

To describe the excess scattering intensity in system I and III at $T < T_c$, in [24] a qualitative

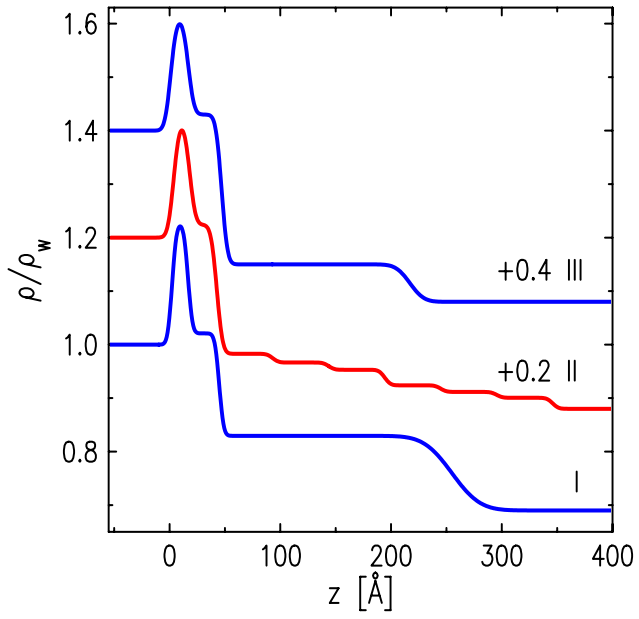


**Fig. 9.** Model profiles of the electron concentration $\langle\rho(z)\rangle$ of the low-temperature phase of the adsorption film of acid-$C_{30}$, normalized to the electron concentration in water under normal conditions $\rho_w = 0.333$ e$^-$/Å$^3$: blue lines – model (13) of systems I and III at $T \approx 288$ K and $T \approx 303$ K, respectively; red line – model (14) of system II at $T \approx 320$ K. For clarity, the numbers near the lines indicate the shift along the vertical axis

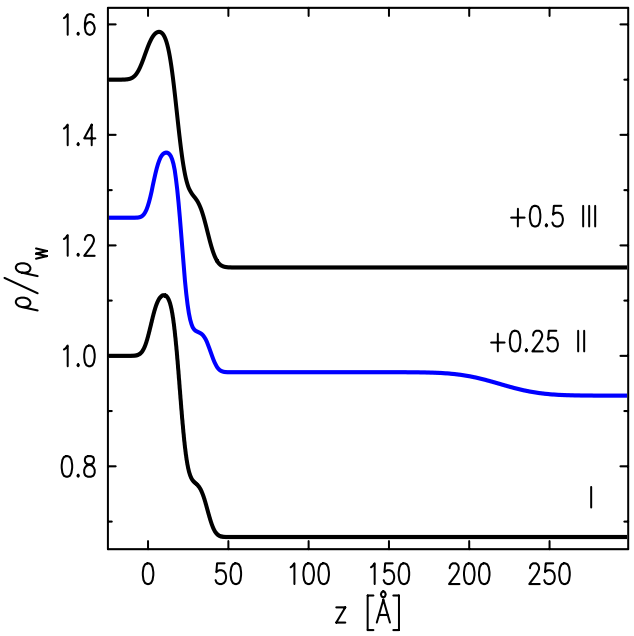


**Fig. 10.** Model profiles of the electron concentration $\langle\rho(z)\rangle$ of the high-temperature phase of the adsorption film of acid–$C_{30}$, normalized to the electron concentration in water under normal conditions $\rho_w = 0.333$ e$^-$/Å$^3$: black lines are model (11) of systems I and III at $T \approx 318$ K and $T \approx 327$ K, respectively; blue line is model (13) of system II at $T \approx 333$ K. For clarity, the numbers near the lines indicate the shift along the vertical axis

three-layer model with a structure factor of the following type was proposed:

$$\Phi(q) = \Phi^*_m(q) + \frac{\delta\rho e^{-\sigma^2 q^2/2}}{\Delta\rho} e^{-iqz_3}. \qquad (13)$$

The second term describes a homogeneous third layer with thickness $z_3 - z_2$ and density $\rho_3 = \rho_h + \delta\rho$ (see Fig. 7). The parameter $\sigma$ – the proper width of the boundary between this layer and the volume of n-hexane $\Phi^*_m(q)$ – is given by expression (11) with the replacement $\rho_3 \to \rho_h + \delta\rho$.

The three-layer model is shown by the blue lines in Fig. 5 for systems I and III and in Fig. 6 for system II. The fitting parameters of the third layer are $z_3 - z_2 \approx 150 \div 200$ Å, the parameter is $\delta\rho \approx 0.05\rho_w \div 0.2\rho_w$, and the width is $\sigma \approx 6 \div 10$ Å ($\sigma > \sigma_R$). A joint analysis of the data for $I_n$ and $R(q_z)$ shows that the contribution of the second term in (13) decreases rapidly with increasing and becomes negligible at $q_z > 0.075$ Å$^{-1}$.

Further, the peaks in the diffuse background and the reflection coefficient for the low-temperature phase in the second type of system are satisfactorily described by a structure factor of the following type [35]:

$$\Phi(q) = \Phi^*_m(q) + \frac{e^{-\sigma_R^2 q^2/2}}{\Delta\rho} \sum_{j=2}^{N} (\rho_{j+1} - \rho_j) e^{-iqz_j}, \qquad (14)$$

where the second term describes the planar layered-periodic (smectic) structure [36] of layer 3 with a period $W = z_{j+1} - z_j$ (for $j \geq 2$), which determines the position of the interference maximum on the scattering curves and the narrow peak in the reflection coefficient. Models with $W = 50 \pm 5$ Å, the number of smectic layers $N - 2 = 6, \ldots, 8$, and $\rho_j - \rho_h < 0.1\rho_w$ (for $j \geq 2$) satisfactorily describe the experimental data for $R(q_z)$ both and $I_n(\beta)$ (red lines in Figs. 5 and 8).

Model profiles of the electron concentration $\langle\rho(z)\rangle$, normalized to the electron concentration in water under normal conditions $\rho_w = 0.333\, e^-$/Å$^3$, of the low-temperature and high-temperature phases of the acid-$C_{30}$ adsorption film for all three systems are presented in Fig. 9 and 10, respectively.

## 5. DISCUSSION

Thus, the soluble adsorption film of acid-$C_{30}$ can be considered as a two-dimensional thermodynamic system with parameters ($p$, $T$, $c$), in which a phase transition is observed with an increase in temperature and constants $p$ and $c$. From observations of lyotropic and thermotropic phase transitions between bulk mesophases in aqueous solutions of fatty acids, one of the parameters determining the thermodynamic state of the system is the pH level of the solution, which affects the degree of ionization of the polar groups of amphiphiles [37, 38]. Thus, the dependences $\gamma(T)$ on the pH level in Fig. 2 are naturally associated with the degree of ionization of the -COOH groups of triacontanoic acid.

It should also be noted that the value of the enthalpy of transition in system II at pH=10 (partially ionized boundary) is eight to nine times less than for system I with pH=2 (protonated boundary). The addition of EDTA to the aqueous subphase leads to an increase $\Delta H$ in system III by two to three times compared to system II and is one third of the value for the protonated system I. The upward shift of the dependences $\gamma(T)$ with increasing pH in system II, in our opinion, is associated with the manifestation of the electrocapillary effect at the n-hexane–water boundary [39]. It should be noted that the observed enthalpy of transition $\Delta H$ for all systems I–III is less than the value of $\approx 1.3$ J/m$^2$ of the enthalpy of the liquid–vapor transition in the adsorption layers of alcohol-$C_{30}$ [40].

The values of the fitting parameters $(\rho_1, \rho_2, l_1, l_2, \sigma_R)$ in model (11) indicate a change in the structure at $T_c$, below which the Gibbs monolayer is in the solid state, and at $T > T_c$ – in the liquid state. The total thickness of the monolayer, $l = 41 \pm 2$ Å ($l = l_1 + l_2$) within the error limits, coincides with the calculated total length of 40.8 Å ($29 \times 1.27$ Å (C-C) + 1.5 Å ($CH_3$) + + 2.5 Å (-COOH)) of the molecule $C_{30}H_{60}O_2$ (contains $\Gamma = 256$ electrons).

Formally, in the low-temperature phase of the monolayer, the area per molecule of acid-$C_{30}$, $\Gamma / (\rho_1 l_1 + \rho_2 l_2) \approx 18$ Å$^2$, differs slightly from the area $\approx 18.4$ Å$^2$ per group -$CH_2$- in the densest crystalline phase of the saturated hydrocarbon [38]. However, the value of the fitting parameter $L_1$ of the model (11) is several times greater than the longitudinal size $\approx 2.5$ Å of the polar group -COOH, and the fitting thickness of the layer of alkyl groups $L_2$ is 9 Å less than the length of the hydrocarbon tail -$C_{29}H_{59}$ (contains $\Gamma_2 = 233$ electrons) of the triacontanoic acid molecule, equal to $l_2^0 \approx 38$ Å. This indicates the presence of an excess electron concentration in the layer of polar groups $\Delta\Gamma$.

If the parameter $\rho_2$ describes the packing density of -$CH_2$- groups with vertical orientation of alkyl tails (of length $l_2^0$), then it corresponds to the area per molecule $A = \Gamma_2 / (\rho_2 l_2^0) = 18.8 \pm 0.5$ Å$^2$. This value is consistent with the diffraction data [41] for both the vertical and canted crystalline phases of the Langmuir monolayer of acid-$C_{30}$ on the water surface, in which the area per molecule is $\approx 18.6$ Å$^2$ and $\approx 19.1$ Å$^2$, respectively. Consequently, there are excess electrons per molecule of the amphiphile at the n-hexane–water $\Delta\Gamma = A(\rho_1 l_1 + \rho_2 l_2) - \Gamma \approx 20$ interface. The value $\Delta\Gamma$ can be associated both with the presence of $SO_4^{2-}$ (50 electrons) and $K^+$ (contains 18 electrons) electrolyte ions in the diffuse part of the surface electric double layer, and with a certain number of $H_2O$ molecules (10 electrons) associated with the polar groups of the monolayer.

It was previously reported for liquid Gibbs monolayers of normal monohydric alcohols at the n-hexane–water interface that the electron concentration in the region of the -$CH_2$-OH head group is 10% higher than in water or in the region of ordered polar groups in Langmuir monolayers of alcohols at the vapor–water interface [42]. The higher density is due to the penetration of water into the region of the head groups in a ratio of one $H_2O$ molecule to three polar groups. The presence of n-hexane molecules in the alkyl part of the monolayer is no more than one molecule per five to six alcohol molecules.

According to molecular dynamics calculations [43], the crystal structure of the neutral triacontanoic acid monolayer at the n-hexane–water interface is stabilized by an extensive network of hydrogen bonds arising between the carbonyl and hydroxyl groups of the molecules of acid-$C_{30}$. The presence in the structure of the "charged" monolayer of electrolyte ions and $H_2O$ molecules associated with the head groups apparently indicates the involvement of the latter in the formation of the hydrogen bond network.

In the high-temperature phase of acid-$C_{30}$, the value of $A = 23 \pm 1$ Å$^2$ corresponds within the error limits to a high-molecular hydrocarbon liquid ($A \approx 23$ Å$^2$) and the parameters of a liquid Gibbs

monolayer of alcohol-$C_{30}$ at the n-hexane–water interface ($A \approx 24$ Å$^2$) [40]. Thus, no significant difference in the hydration of liquid monolayers of acid-$C_{30}$ and alcohol-$C_{30}$ is observed experimentally.

On the one hand, in the solid phase $T < T_c$ of systems I and III the observed scattering intensity at small β is more than one order of magnitude higher than the non-specular scattering background from the monolayer (solid black lines in Figs. 5 and 6) and is practically independent of temperature up to $T_c$. On the contrary, in the liquid phase of the monolayer at $T$ above a certain temperature $T^*$ the experimental scattering data are well described by scattering on a liquid Gibbs monolayer with parameters established from reflectometry data. Thus, at $T_c < T < T^*$ scattering occurs on a structure more complex than a homogeneous monolayer, and the thermotropic transition from the surface phase with a solid monolayer to the phase with a liquid monolayer occurs in two stages with temperatures $T_c$ and $T^*$ (see Fig. 11 *a*). Moreover, if the melting of the monolayer in $T_c$ occurs in a sufficiently narrow vicinity of $\Delta T \leq 0.2$ K [24], then the evaporation of the extended layer 3 is delayed in the temperature range $T^* - T_c \geq 20$ K.

On the other hand, according to experimental data for a type II system [35], during the "freezing" of the interphase boundary, in addition to the crystallization of the Gibbs monolayer in an adsorption film of thickness up to $\sim 400$ Å, a planar smectic structure [36] of layers of thickness $\sim 50$ Å is formed (see Fig. 11 *b*). With an increase in temperature at $T = T_c$, the monolayer melts, and the smectic structure disappears. However, the high level of intensity of non-specular scattering in the low-temperature phase indicates the presence of a sufficiently extended near-surface disordered layer in the entire accessible temperature range. The protracted nature of the evaporation of layer 3 in systems I–III possibly reflects the formal prohibition of a first-order transition (abrupt transition) in the electrical double layer at the liquid–liquid interface [44].

In system III, EDTA molecules in the aqueous medium of the subphase bind metal ions into stable complexes and thereby prevent their interaction with the adsorption film of acid-$C_{30}$ [18]. Then, from a comparison of the scattering curves in Figs. 5 and 6 for systems II and III, it immediately follows that potassium cations $K^+$ also participate

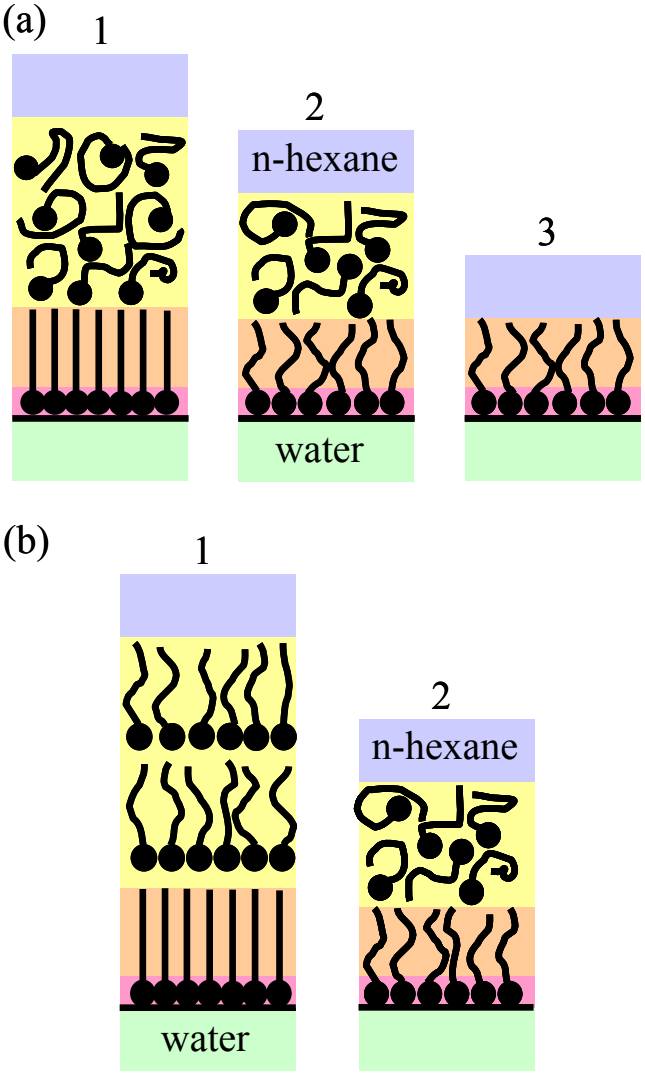


**Fig. 11.** Structures of the adsorbed layer of triacontanoic acid $C_{30}H_{60}O_2$ at the n-hexane–water interface. *a* – Transverse structure of the n-hexane–water interface for systems I and III: 1 – thick layer with a crystalline monolayer at $T < T_c$; 2 – layer with a liquid monolayer in the intermediate region $T_c < T < T^*$; 3 – homogeneous liquid monolayer at $T > T^*$. *b* – Transverse structure of the n-hexane–water interface for system II: 1 – thick film with a crystalline monolayer and a smectic layer at $T < T_c$; 2 – layer with a liquid monolayer at $T > T_c$

in the formation of a smectic superstructure in the extended layer 3 of the film, which, according to the scattering data, is not formed in systems I and III.

Moreover, since the parameter $c$ is the same for all systems, it also follows from the data presented in Fig. 2 that the concentration of metal ions $K^+$ in the aqueous phase significantly affects not only the value of $\Delta H$, but also $T_c$. The discrepancies in the values $T_c$ for systems I and III are possibly also due

to the presence of a certain amount of free cations $K^+$ in the subphase of system III.

Finally, in the qualitative models considered, expression (10) describes the width of the boundaries between the layers. Analysis of the data for systems I and III shows that the boundary between the extended layer 3 and the bulk oil phase is described by a width $\sigma$ two to three times greater than $\sigma_R$, which apparently indicates the presence of an intrinsic structure of a noncapillary-wave nature. This is possible, for example, if the component of grazing small-angle scattering $I_n$ on inhomogeneities of the near-surface layer makes a significant contribution to the intensity of surface scattering [45, 46]. In this case, the study of the spectral properties of the correlation function of the interphase boundary heights requires separate consideration, which is beyond the scope of this work.

Thus, the work systematizes the available data on interfacial tension and X-ray scattering measurements in the vicinity of the solid–liquid thermotropic phase transition in the soluble adsorption film of triacontanoic acid at the n-hexane–water interface in systems with different chemical compositions of the background electrolyte in the aqueous subphase. A qualitative three-layer model is considered that consistently describes the reflectometry and non-specular scattering data for both phases. With increasing temperature, the reversible rearrangement of the adsorption film structure (of thickness $200 \div 400$ Å) at the interface occurs in two stages. At the first stage, in a narrow temperature range of $\Delta T \leq 0.2$ K in the vicinity $T_c$, the melting transition of the solid Gibbs monolayer of thickness $41 \pm 2$ Å and area per molecule $A = 18.8 \pm 0.5$ Å$^2$ into a liquid monolayer of thickness $36 \pm 3$ Å ($A = 23 \pm 1$ Å$^2$) occurs. A further increase in temperature leads to a decrease in the film thickness (its evaporation) down to a thickness of one liquid monolayer. This process occurs in a wide temperature range $\geq 20$ K. According to experimental data $T_c$, $\Delta H$ and the structure of the adsorption films of acid-$C_{30}$ are determined by the composition of the background electrolyte in the aqueous subphase. In the solid phase of the monolayer, an excess electron concentration is observed, which, in our opinion, is associated with the addition of electrolyte ions and water molecules to the polar group of the lipid.

## FUNDING

The NSLS synchrotron was supported by the U.S. Department of Energy under contract No. DE-AC02-98CH10886. The X19C station was funded by ChemMatCARS, the University of Chicago, the University of Illinois at Chicago, and Stony Brook University. The work was supported by the Ministry of Science and Higher Education of the Russian Federation as part of the work on the State assignment of the IPP RAS. The theoretical part of the work (Sects. 3–5) was supported by a grant from the Russian Science Foundation (project No. 23-12-00200).

## REFERENCES

1. *J.W. Gibbs*, Collected Works, Vol. 1: Thermodynamics. New York: Dover, 1961. P. 219.
2. *L.D. Landau and E.M. Lifshitz*, Course of Theoretical Physics, Vol. 5: Statistical Physics (Nauka, Moscow, 1995; Pergamon, Oxford, 1980).
3. *S.V. Kiriyan and B.A. Altoiz*, Tr. MFTI **2** (2), 101 (2010).
4. *R.Z. Safieva*, Petroleum Physical Chemistry: Physicochemical Principles of Oil Processing Technology (Khimiya, Moscow, 1998) [in Russian].
5. *K. Akbarzadeh*, *A. Hammami*, *A. Kharrat*, *D. Zhan*, *S. Allenson*, *J. Creek*, *S. Kabir*, *A.J. Jamaluddin*, *A.G. Marshall*, *R.P. Rodgers*, *O.C. Mullins*, *T. Solbakken*, Oilfield Review 19(2), 22 (2007).
6. *G. Gouy*, J. Phys. **9**, 457 (1910).
7. *D.L. Chapman*, Phil. Mag. **25**, 475 (1913).
8. *J.C. Earnshaw and C.J. Hughes*, Phys. Rev. A **46**, R4494 (1992).
9. *X.Z. Wu*, *E.B. Sirota*, *S.K. Sinha*, *B.M. Ocko*, *and M. Deutsch*, Phys. Rev. Lett. **70**, 958 (1993).
10. *J.T. Davies*, *E.K. Rideal*, Interfacial Phenomena, Academic Press, New York, 1963.
11. *D.M. Mitrinovic*, *A.M. Tikhonov*, *M. Li*, *Z. Huang*, *and M.L. Schlossman*, Phys. Rev. Lett. **85**, 582 (2000).
12. *Q. Lei*, *C.D. Bain*, Phys. Rev. Lett. **92**, 176103 (2004).
13. *L. Tamam*, *D. Pontoni*, *Z. Sapir*, *Sh. Yefet*, *E. Sloutskin*, *B.M. Ocko*, *H. Reichert*, *and M. Deutsch*, PNAS **108**, 5522 (2011).
14. *A.M. Tikhonov*, JETP Lett. **102**, 552 (2015).
15. *A.M. Tikhonov*, *V.E. Asadchikov*, *Yu.O. Volkov*, *A.D. Nuzhdin*, *B.S. Roshchin*, Instruments and Experimental Techniques **64**(1), 172 (2021).
16. *A. Goebel*, *K. Lunkenheimer*, Langmuir **13**, 369 (1997).

**17**. *T. Takiue*, *A. Yanata*, *N. Ikeda*, *K. Motomura*, *M. Aratono*, J. Phys. Chem. **100**, **13743**, (1996).

**18**. *J.R. Hart*, Ullmann's Encyclopedia of Industrial Chemistry, Wiley-VCH Verlag GmbH & Co. KGaA, Weinheim, **573**, 2011.

**19**. *A.W. Adamson*, Physical Chemistry of Surfaces, 3rd ed.; John Wiley & Sons: New York, 1976.

**20**. *M.L. Schlossman*, *D. Synal*, *Y. Guan*, *M. Meron*, *G. Shea-McCarthy*, *Z. Huang*, *A. Acero*, *S.M. Williams*, *S.A. Rice*, *P.J. Viccaro*, Rev. Sci. Instrum. **68**, 4372 (1997).

**21**. *F.A. Akin*, *I. Jang*, *M.L. Schlossman*, *S.B. Sinnott*, *G. Zajac*, *E.R. Fuoco*, *M.B. J. Wijesundara*, *M. Li*, *A.M. Tikhonov*, *S.V. Pingali*, *A.T. Wroble*, *L. Hanley*, J. Phys. Chem. B **108**, 9656 (2004).

**22**. *A.M. Tikhonov*, JETP Lett. **92**, 356 (2010).

**23**. *M.L. Schlossman*, *M. Li*, *D.M. Mitrinovic*, *A.M. Tikhonov*, High Performance Polymers **12**, 551 (2000).

**24**. *A.M. Tikhonov*, JETP Lett. **104**, 309 (2016).

**25**. *Y. Yoneda*, Phys. Rev. **131**, 2010 (1963).

**26**. *S.K. Sinha*, *E.B. Sirota*, *S. Garoff*, *and H.B. Stanley*, Phys. Rev. B **38**, 2297 (1988).

**27**. *V. Holy*, *T. Baumbach*, Phys. Rev. B **49**, 10668 (1993).

**28**. *F.P. Buff*, *R.A. Lovett*, *F.H. Stillinger*, Phys. Rev. Lett. **15**, 621 (1965).

**29**. *A. Braslau*, *P.S. Pershan*, *G. Swislow*, *B.M. Ocko*, *and J. Als-Nielsen*, Phys. Rev. A **38**, 2457 (1988).

**30**. *D.K. Schwartz*, *M.L. Schlossman*, *E.H. Kawamoto*, *G.J. Kellogg*, *P.S. Pershan*, *B.M. Ocko*, Phys. Rev. A **41**, 5687 (1990).

**31**. *D.M. Mitrinovic*, *S.M. Williams*, *M.L. Schlossman*, Phys. Rev. E **63**, 021601 (2001).

**32**. *J.D. Weeks*, J. Chem. Phys. **67**, 3106 (1977).

**33**. *A. Braslau*, *M. Deutsch*, *P.S. Pershan*, *A.H. Weiss*, *J. Als-Nielsen*, *J. Bohr*, Phys. Rev. Lett. **54**, 114 (1985).

**34**. *A.M. Tikhonov*, J. Chem. Phys. **130**, 024512 (2009).

**35**. *A.M. Tikhonov*, JETP Lett. **105**, 775 (2017)**.**

**36**. *P.S. Pershan*, Physics Today **35**, **5**, 34 (1982).

**37**. *D.P. Cistola*, *D.M. Small*, *J.A. Hamilton*, J. Lipid Res. **23**, 795 (1982).

**38**. *D.M. Small*, The Physical Chemistry of Lipids, Plenum Press, New York, 1986.

**39**. *L.D. Landau*, *E.M. Lifshitz*, Course of Theoretical Physics, Vol. 8: Electrodynamics of Continuous Media, 2nd ed.; Pergamon: New York, 1984.

**40**. *A.M. Tikhonov*, *M.L. Schlossman*, J. Phys. Chem. B. **107**, 3344 (2003).

**41**. *D. Jacquemain*, *F. Leveiller*, *S.P. Weinbach*, *M. Lahav*, *L. Leiserowitz*, *K. Kjaer*, *J. Als-Nielsen*, J.Am. Chem. Soc. **113** (20), 7684 (1991).

**42**. *A.M. Tikhonov*, *S.V. Pingali*, *and M.L. Schlossman,* J. Chem. Phys. **120**, 11822 (2004).

**43**. *A.M. Tikhonov*, *H. Patel*, *S. Garde*, *and M.L. Schlossman*, J. Phys. Chem. B. **110**, 19093 (2006).

**44**. *V.I. Marchenko*, *Zh. Éksp.* Teor. Fiz. **81** (3), 1142 (1981) [Sov. Phy. JETP 54 (3), 605 (1981)].

**45**. *M. Li*, *A.M. Tikhonov*, *M.L. Schlossman*, J. Europhys. Lett. **58**, 80 (2002).

**46**. *A.M. Tikhonov*, *Yu.O. Volkov*, ZhETF, Vol. **165**, No. **4**, p. 486